JOURNAL OF APPLIED ELECTROCHEMISTRY 12 (1982) 743–757

Anodic dissolution of n-type and p-type chalcopyrite

R. S. McMILLAN*, D. J. MacKINNON and J. E. DUTRIZAC

Mineral Sciences Laboratories, CANMET, Energy, Mines and Resources Canada, 555 Booth St., Ottawa, Ontario, K1A 0G1, Canada

Received 4 March 1982

The anodic dissolution of n- and p-type chalcopyrite ($CuFeS_2$) was studied in both acidic sulphate and acidic chloride media under conditions relevant to chemical leaching, i.e., at temperatures $> 70°C$ and over the potential region 0.2–0.6 V versus SCE. Double potential pulse chronoamperometry was used to probe the surface of the chalcopyrite anodes to determine the activation currents at various applied overpotentials. Analysis of the data obtained in both systems indicated the formation of a surface layer, a solid electrolyte interphase (SEI), which slows the rate of electron transfer. The electron transfer between various redox couples, including Cu^{2+}/Cu^{+}, Fe^{3+}/Fe^{2+} and I_3^-/I^- on n- and p-type chalcopyrite and on Pt, was compared using cyclic voltammetry. In the potential region of interest, the Fe^{3+}/Fe^{2+} couple is much less reversible on chalcopyrite than are the Cu^{2+}/Cu^{+} and I_3^-/I^- redox couples. Chemical leaching of chalcopyrite in the presence of various oxidants was also carried out, and the results of the chemical experiments were discussed in terms of the electrochemical properties of the systems.

1. Introduction

Recently a number of studies on the electrochemical behaviour of chalcopyrite ($CuFeS_2$) under conditions comparable to those encountered during chemical leaching have been published [1–5]. Because of the strong evidence that the reactions occurring during leaching are, at least in part, electrochemical in nature [1, 2], it was felt that such studies could provide further insight into the mechanisms involved in chalcopyrite dissolution. In spite of this recent research, however, the electrochemistry of chalcopyrite is not completely understood and many of the experimental results have yet to be adequately explained.

Linge [6] postulated that a layer of metal deficient material is formed during the initial leaching of chalcopyrite in ferric solutions and that this layer rapidly builds up to a limiting thickness of about 5 nm. Both Linge [6] and Bauer *et al.* [7] have shown that the chemical leaching of chalcopyrite occurs initially with the selective dissolution of iron; the shorter the time of measurement the higher the Fe/Cu ratio in solution. Warren [5], Parker *et al.* [1, 2] and Jones [4] arrived at the same conclusions based on the results of their studies on the anodic dissolution of chalcopyrite.

Parker *et al.* [1, 2] observed two distinct regions during the slow potential scan of a chalcopyrite anode. From potentials of 0.2 to ~0.6 V versus SCE the current density was $< 1\ mA\ cm^{-2}$, was dependent on pH and temperature, and slowly increased with increasing potential. Over this potential range, the main oxidation products were Fe^{2+}, Cu^{2+} (Cu^{+} in chloride medium) and S^0. At potentials > 0.6 V versus SCE the current increased rapidly with increasing potential and the main oxidation products were Fe^{3+}, Cu^{2+} and SO_4^{2-}. The current–time dependence at constant potential observed by Parker *et al.* [1, 2] indicated that the rate of chalcopyrite dissolution was being retarded by diffusion of products through a slowly thickening layer. Based on the results of ring-disc experiments they concluded that the passivating layer consisted of a copper-bearing species and suggested a copper polysulphide (CuS_x, where $x > 2$).

Jones and Peters [4] suggested that CuS (covellite) is formed in the low current region during the anodic dissolution of chalcopyrite. Ammou [3] studied the electro-oxidation of chalcopyrite in acid chloride solution and proposed a mechanism

*Present Address: Department of Physics, University of British Columbia, Vancouver, B.C. V65 2A6, Canada.

0021-891X/82/060743-15$04.30/0

involving the formation of CuS to explain the decrease in rate of electrodissolution. The formation of CuS was thought to be responsible for the superficial enrichment of the solid surface in copper as well as for the retardation of the Fe^{2+} solubilization rate. Ammou concluded that CuS covered the chalcopyrite–electrolyte interface by accumulating in the porous sulphur network which formed a gradually thickening layer at the surface. The CuS gradually blocked the pores of the sulphur network resulting in a decrease in the reaction area and hence in the dissolution rate. The next step in the dissolution sequence is the oxidation of interstitial CuS at the solid–solution interface that controls the overall long term reaction rate.

In the present study the investigations of chalcopyrite were extended to include both n- and p-type material, to obtain more detailed information on the semiconducting properties of chalcopyrite, and to relate these data to the results of electrochemical dissolution as well as to chemical leaching in the presence of various oxidants.

2. Experimental procedure

A variety of electrochemical methods including linear sweep voltammetry, cyclic voltammetry, galvanstatic pulse chronopotentiometry and double potential step chronoamperometry were employed using conventional instrumentation. Double potential step chronoamperometry is a non-stationary technique which does not significantly alter the surface of the chalcopyrite, thus enabling data to be obtained in the absence of a product layer or for a product layer of constant thickness. The experimental set-up for the application of double potential step chronoamperometry is also fairly conventional. It includes a square wave pulse generator to provide potential pulses of varying magnitude, a scan generator to provide a constant zero overpotential, a potentiostat with IR compensation that can handle rapid rise times and a storage oscilloscope to facilitate recording of current transients. This technique was applied in this study as follows. A potential pulse of increasing magnitude was applied from the rest potential, or zero overvoltage ($\eta = 0$) for 30 ms; the time between pulses was 60 s which was sufficient for the chalcopyrite surface to relax to its steady state condition. The resulting current transients, I_1, I_2, etc., were recorded on the storage oscilloscope.

The electrodes were prepared from natural specimens of massive chalcopyrite obtained from Messina, Transvaal, South Africa and from Kidd Creek Mines Limited, Timmins, Ontario, Canada. The specimens were cut into cubes (~ 1 cm edges) and were mounted in epoxy with an electrical contact silver epoxied to the back face. The back face of the mounted specimen was threaded to a plexiglass shaft which could be attached to a stirring motor. The exposed face of the electrode was ground and then polished on 600 grit silicon carbide paper followed by 0.3 μm alumina.

The elemental analyses of the bulk chalcopyrite samples are listed below.

	Transvaal wt%	*Timmins* wt%
Cu	35.3	36.3
Fe	30.1	30.1
S	34.7	29.6
Ag	5.5 ppm	117 ppm
Cu/Fe	1.03	0.93
Cu/S	0.51	0.55

The relative proportions of the constituent minerals as determined by Quantimet image analysis are:

	Transvaal wt%	*Timmins* wt%
Chalcopyrite	98.2	81.9
Pyrite	0.1	8.1
Pyrrhotite	–	0.2
Sphalerite	–	1.1
Silicates	1.7	8.7

Note that the Transvaal material is the purer and that it is nearly stoichiometric; the Timmins material is high in silver. The electrical properties, including Hall coefficients and semiconductor type, were also determined [8] for both types of chalcopyrite and are presented in Table 1. Room temperature Hall measurements and thermoelectric power (hot probe) measurements showed the Transvaal samples to be predominantly p-type but the Timmins samples were n-type semiconduc-

Table 1. Electrical properties of the chalcopyrite specimens

	Transvaal	*Timmins*
ρ (ohm cm)	7.9	0.12
μ_H ($cm^2 V^{-1} s^{-1}$)	11.5	2.2
R_H ($cm^3 C^{-1}$)	+83	−0.26
n(p) (cm^{-3})	$p = 7.4 \times 10^{16}$	$n = 2.4 \times 10^{19}$
	$n = 7.7 \times 10^{15}$	$p = 2.4 \times 10^{13}$
	$N_c \sim N_v \sim 4 \times 10^{20}$	–
	$N_i \sim 2 \times 10^{16}$	–
E_g (eV)	~0.5	~0.5

tors. The carrier concentrations for the p-type (Transvaal) chalcopyrite are so low that it is not a degenerate semiconductor and thus should not act as a metal electrode under any conditions of potential bias. The n-type (Timmins) chalcopyrite is sufficiently close to being degenerate that it should act as a metal electrode.

A three electrode thermostated glass cell with a large Pt-black mesh counter electrode and an isolated reference (standard silver electrode, SSE) was used. Ionic conductance from the SSE to the chalcopyrite working electrode was via a Luggin capillary. All potentials are reported with respect to the standard hydrogen electrode (SHE). Both 0.3 mol dm^{-3} H_2SO_4 and 0.3 mol dm^{-3} HCl electrolytes were used. Oxygen was purged from the solution with a nitrogen stream although preliminary experiments showed no rate dependence on added oxygen or on electrode rotation speeds up to 3000 rpm. The chalcopyrite electrodes were equilibrated in the electrolyte for 20 min prior to initiating an experiment.

Chemical leaching experiments were also carried out to illustrate the importance of chemical oxidation potential on the long-term dissolution of chalcopyrite and to try to shed further light on the relative behaviour of the different oxidants. All work was done with 1 g of −29, +20 μm Transvaal chalcopyrite of the purity indicated above. Leaching was done at 90° C using 2.7 dm^{-3} of lixiviant held in a thermostated water bath; the tests were run under a protective nitrogen cover. Solutions of differing oxidizing potential were prepared from the various oxidants, and 0.5 g dm^{-3} of the appropriate reduced species was added to 'buffer' the system against abrupt changes in oxidation potential. The oxidation potentials of the various solutions were measured at 90° C before and after the tests using both chalcopyrite and platinum electrodes. The course of the leaching reaction was followed by taking samples at regular intervals and subsequently by analyzing these for copper using atomic absorption spectroscopy. Initial leaching rate constants were derived from the initial slopes of the leaching curves and these constants were then compared to the electrochemical properties of the lixiviant. Details of the chemical leaching procedure for chalcopyrite have been presented previously [9].

3. Results and discussion

3.1. *Electrochemical behaviour of chalcopyrite*

Linear polarization curves for the Transvaal chalcopyrite (p-type), the Timmins chalcopyrite (n-type) and Pt obtained in 0.3 mol dm^{-3} HCl at 25° C at a potential scan rate of 0.1 V s^{-1} are compared in Fig. 1. On the positive going scan, both chalcopyrite electrodes exhibit a region of low current from the rest potential ($E_R \simeq 0.5$ V versus SHE) to about 1.3 V versus SHE, followed by a region of high current ($E > 1.3$ V versus SHE). The potential at which the high current region occurs is variable and depends on both pH and temperature. The current obtained for the n-type chalcopyrite is $\simeq 3.3$ times greater than that obtained for the p-type chalcopyrite at the same potential. Similar results were obtained in 0.3 mol dm^{-3} H_2SO_4 electrolyte. The results presented in the following sections of this paper will be focused on the low anodic current region; i.e., from the rest potential to $\simeq 1.3$ V versus SHE since this is the

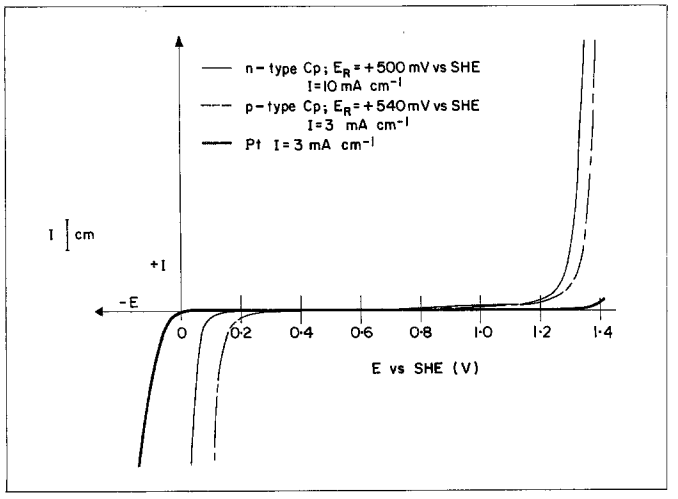

Fig. 1. Linear polarization curves obtained in 0.3 mol dm^{-3} HCl at 25°C using various electrodes. Scan rate, 0.1 V s^{-1}.

potential range in which the common chemical leachants such as ferric or cupric ion are active.

When the chalcopyrite electrode is initially placed in the electrolyte on open circuit, it establishes a rest potential, E_R. In this case, the rest potential rapidly increases to more positive potentials during the first five minutes of immersion. By the end of the 20 min equilibration period, the rest potential has reached a steady value. The equilibrated rest potential is dependent on the temperature and on the type of electrolyte; it can vary by ±40 mV.

3.2. *Application of double potential step chronoamperometry*

3.2.1. *General.* Current transients resulting from the application of a double potential pulse of 30 ms to the chalcopyrite electrode are shown in Fig. 2 (a) and (b). These current transients are typical of those obtained from either 0.3 mol dm^{-3} HCl or 0.3 mol dm^{-3} H_2SO_4 electrolyte over the temperature range 25–90° C. Fig. 2(a) shows the result obtained on a freshly polished, equilibrated surface over the overpotential range 20–600 mV. There is an initial capacitance charging current followed by a faradaic reaction for which the current decays with time.

Figure 2(b) shows the current transient obtained for overpotentials > 600 mV; there is no longer a decay of current with time. This behaviour occurs in the high current region; i.e., $E >$ 1.3 V versus SHE (see Fig. 1). A visual examination of the chalcopyrite surface after a series of

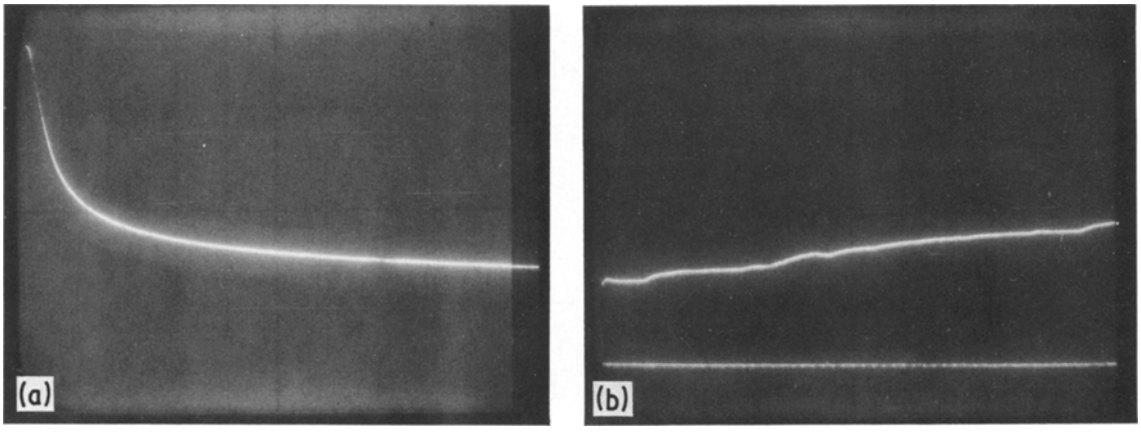

Fig. 2. Current transients resulting from the application of a double potential step of 30 ms to the chalcopyrite; y-axis is current (mA) and x-axis is time (ms) (a) freshly polished and equilibrated chalcopyrite for overpotentials < 600 mV versus SHE, (b) freshly polished and equilibrated chalcopyrite for overpotentials > 600 mV versus SHE.

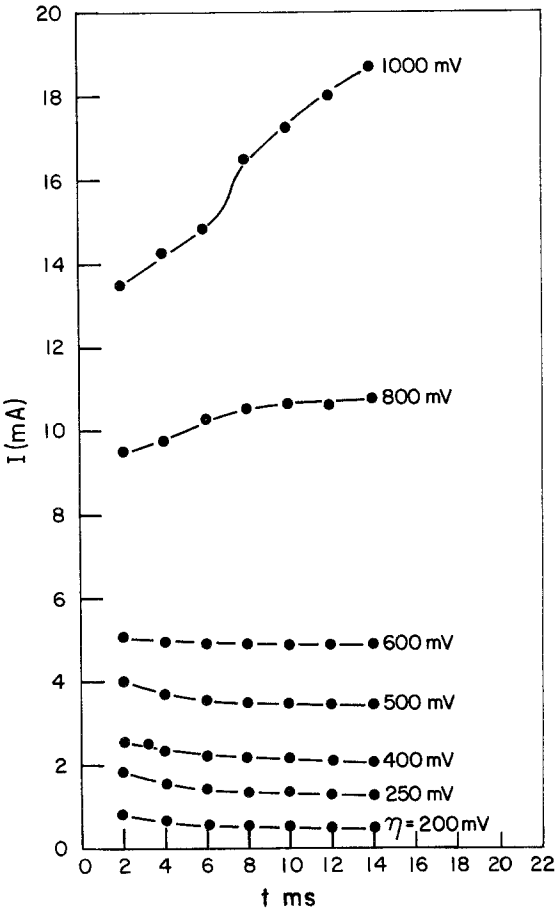

Fig. 3. Current versus time curves obtained from the double potential step experiments on p-type chalcopyrite equilibrated in 0.3 mol dm^{-3} H_2SO_4–0.2 mol dm^{-3} NaCl at 50° C. V_R = + 580 mV versus SHE.

overpotential pulses reveals a thin blue product layer which suggests a 'copper-rich' sulphide phase.

Figure 3 shows a series of current–time plots obtained from a typical double potential pulse experiment for overpotentials from 200–1000 mV. These results are for p-type chalcopyrite in 0.3 mol dm^{-3} H_2SO_4 at 50° C and clearly show that for $\eta < 600$ mV, the current decays with time, but for $\eta > 600$ mV, it increases with time.

3.2.2. Analysis of current transients. Fig. 4 shows a plot of current I versus $t^{1/2}$ for the data given in Fig. 3. The linear relationship observed (η = 200–600 mV) indicates that the equation [10]:

$$I = I_{act}\left(1 - \frac{2kt^{1/2}}{D_m^{1/2}}\right) \qquad (1)$$

is obeyed and hence the anodic dissolution of chalcopyrite is irreversible. In the equation, D_m is the diffusion coefficient for an active species, k the overall rate constant for the oxidation reaction and I_{act} is the diffusion-free activation current which can be obtained from the $t^{1/2} = 0$ intercept of the plots shown in Fig. 4. The I_{act} values can be plotted versus overpotential η in accordance with the Tafel equation

$$I_{act} = I_0 \exp\left(\frac{\alpha n F \eta}{RT}\right) \qquad (2)$$

from which the values of I_0 (exchange current density) and αn (where α is the oxidation transfer coefficient and n is the number of electrons transferred in the rate determining step) can be obtained. These parameters can be useful quantities for determining the mechanism of an electrochemical reaction.

Tafel plots ($\log I$ versus η) obtained from data taken from current transients on freshly polished and equilibrated p-type chalcopyrite in 0.3 mol dm^{-3} H_2SO_4 at various temperatures are shown in Fig. 5. Similar plots were obtained using 0.3 mol dm^{-3} HCl electrolyte. Values of I_0 were obtained from the $\eta = 0$ intercept and αn values were derived from the slope of the Tafel plots. At low overvoltages, the Tafel relation no longer applies since I_{act} is linear with η according to the equation [11]:

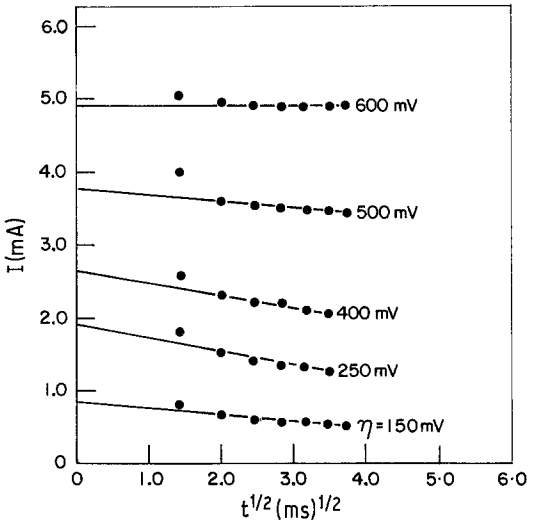

Fig. 4. Current versus square root time curves derived from the data of Fig. 5 for p-type chalcopyrite at 50° C. V_R = + 580 mV versus SHE.

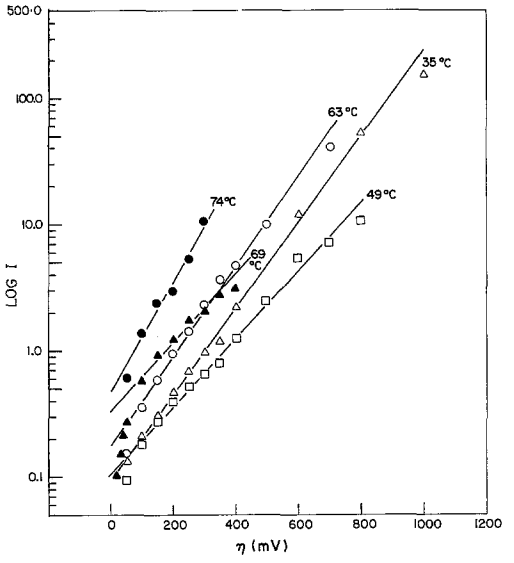

Fig. 5. Anodic Tafel plots obtained on freshly polished p-type chalcopyrite in 0.3 mol dm^{-3} H_2SO_4 media. V_R = + 580 mV versus SHE.

$$I_{act} = I_0 \frac{nF}{RT} \eta \qquad (3)$$

from which values of n can be obtained.

Experiments were also done in which the chalcopyrite electrode was held at $\eta = 600$ mV for 45 min at the temperature of interest to allow a significant product layer to form on the surface. The Tafel plots shown in Fig. 6 were obtained as a result of applying the double potential pulse to this type of surface. The data shown are for 0.3 mol dm^{-3} H_2SO_4 electrolyte and the plots indicate higher Tafel slopes and an abnormal temperature dependence of I_0 as compared to the results obtained in the absence of a significant product layer, see Fig. 5. The results obtained similarly for the chalcopyrite electrode poised potentiostatically in 0.3 mol dm^{-3} HCl electrolyte also show higher Tafel slopes but the temperature dependence of I_0 was normal; i.e., I_0 increased with increasing temperature.

Values of I_0, the exchange current density, are plotted according to the Arrhenius equation in Fig. 7 for 0.3 mol dm^{-3} HCl electrolyte and in Fig. 8 for 0.3 mol dm^{-3} H_2SO_4 electrolyte. For the 0.3 mol dm^{-3} HCl electrolyte, the Arrhenius plots, Fig. 7, yield a linear region from 50 to 78° C. The slope of the line gives an activation enthalpy, ΔH^0, which for freshly polished and equilibrated surfaces is 48.5 ± 8.8 kJ $mole^{-1}$; ΔH^0 for the surface containing the product layer is 64.4 ±

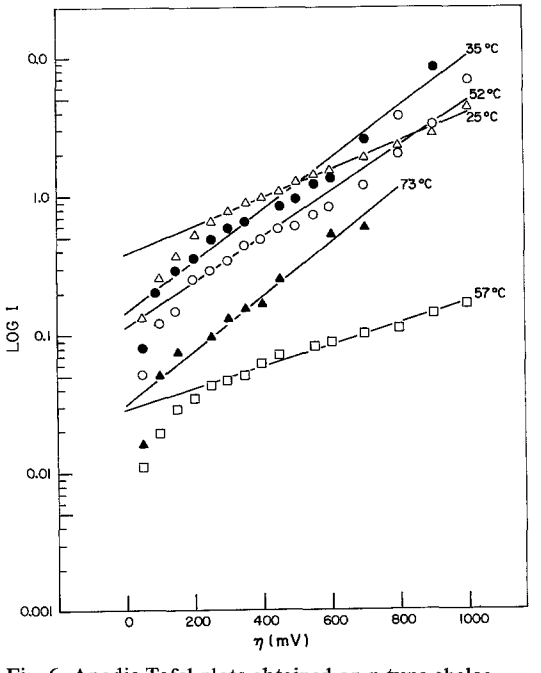

Fig. 6. Anodic Tafel plots obtained on p-type chalcopyrite containing a significant product layer, in 0.3 mol dm^{-3} H_2SO_4 media. V_R = + 700 mV versus SHE.

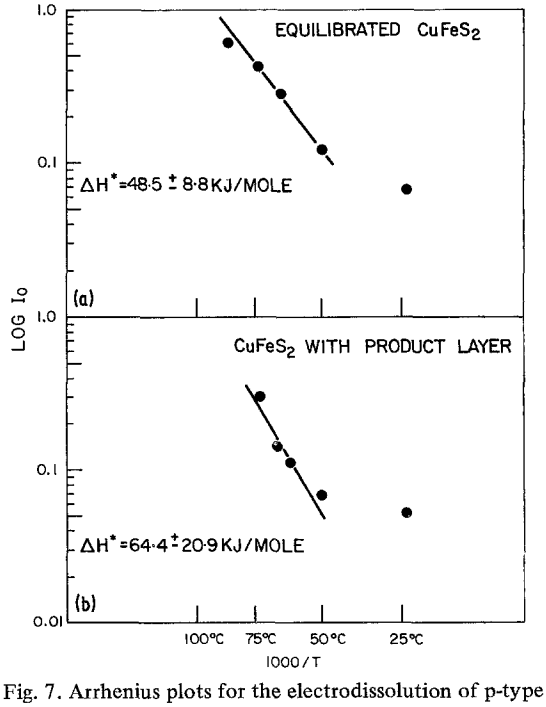

Fig. 7. Arrhenius plots for the electrodissolution of p-type chalcopyrite in 0.3 mol dm^{-3} HCl media. (a) V_R = + 540 mV versus SHE, (b) V_R = + 700 mV versus SHE.

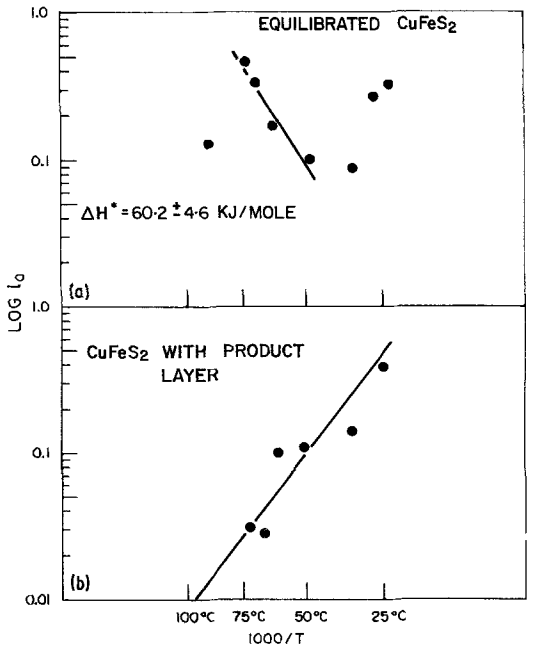

Fig. 8. Arrhenius plots for the electrodissolution of p-type chalcopyrite in 0.3 mol dm^{-3} H_2SO_4 media. V_R = + 540 mV versus SHE.

20.9 kJ $mole^{-1}$. These two values are in reasonable agreement, considering the experimental error, and indicate that similar reactions are occurring on the two types of surface. These values of ΔH^0 are similar to those obtained for chemical leaching of chalcopyrite in $FeCl_3$ media.

A linear Arrhenius region was also observed between 50–74° C for anodic dissolution of p-type chalcopyrite in 0.3 mol dm^{-3} H_2SO_4 and yielded a ΔH^0 value of 60.2 ± 4.6 kJ $mole^{-1}$. In the 0.3 mol dm^{-3} H_2SO_4 electrolyte for temperatures $<50°$ C or $>74°$ C, anomalous behaviour occurs even in the absence of an extensive product layer, Fig. 8, indicating a different reaction surface or dissolution process. The presence of a product layer in 0.3 mol dm^{-3} H_2SO_4 electrolyte results in a completely anomalous Arrhenius behaviour, Fig. 8, again suggesting that the reaction or the reaction surface is different than that existing in the 0.3 mol dm^{-3} HCl electrolyte.

The data obtained from the current transient experiments for p-type chalcopyrite in 0.3 mol dm^{-3} HCl and 0.3 mol dm^{-3} H_2SO_4 are summarized in Tables 2 and 3, respectively. In 0.3 mol dm^{-3} HCl, for the freshly polished, equilibrated electrode, Tafel slopes of $\simeq$ 200 mV/decade, n values of $\simeq 0.8$ and αn values of $\simeq 0.3$ were obtained. In the presence of a significant product layer, the Tafel slopes increased to $\simeq$ 400 mV/decade, n was reduced to $\simeq 0.4$ and αn decreased to $\simeq 0.2$. In addition, in 0.3 mol dm^{-3} HCl in both cases, i.e., with a thin product layer or a thicker product layer, the temperature dependence of the Tafel slopes is not that predicted; i.e., a linear dependence of slope with temperature was not observed. In fact the Tafel slopes are relatively insensitive to temperature. Similar results are found in 0.3 mol dm^{-3} H_2SO_4 although the Tafel slopes are higher than in 0.3 mol dm^{-3} HCl. These observations coupled with low n and αn values suggest a complex dissolution process at the chal-

Table 2. Kinetic data for the anodic dissolution of p-type chalcopyrite in 0.3 mol dm^{-3} HCl

T (° C)	I_0 (mA)	*Tafel slope* (mV/decade)	$n = \frac{2aZ}{y}$	$\alpha\eta = \frac{aZ}{Y}$	ΔH^0 (kJ $mole^{-1}$)
0.3 mol dm^{-3} HCl equilibrated electrode					
23.5	0.066	186	1.01	0.32	48.5
50.0	0.12	255	0.84	0.25	50–87°C
63.0	0.28	202	0.83	0.33	
74.0	0.44	225	0.69	0.31	
87.0	0.59	213	0.87	0.34	
After 45 min anodic dissolution					
23.5	0.051	508	0.46	0.12	64.4
50.0	0.068	444	0.45	0.14	50–74°C
62.5	0.11	430	0.39	0.29	
67.0	0.14	295	0.54	0.23	
73.5	0.30	332	0.56	0.21	

Table 3. Kinetic data for the anodic dissolution of p-type chalcopyrite in 0.3 mol dm^{-3} H_2SO_4

T (°C)	I_0 (mA)	*Tafel slope* (mV/decade)	$n = \frac{2aZ}{Y}$	$\alpha\eta = \frac{aZ}{Y}$	ΔH^0 (kJ mole^{-1})
0.3 mol dm^{-3} H_2SO_4 equilibrated electrode					
23.5	0.32	266	0.53	0.22	60.2
28.0	0.27	359	0.37	0.17	50–75°C
35.0	0.089	291	0.78	0.21	
49.0	0.10	373	0.50	0.17	
63.0	0.17	273	0.51	0.24	
69.0	0.33	369	0.46	0.18	
74.0	0.46	229	0.78	0.30	
80.0	0.03	338	0.53	0.21	
88.0	0.13	179	1.08	0.40	
After 45 min anodic dissolution					
25.0	0.38	1025	0.18	0.06	
35.0	0.14	536	0.30	0.11	
52.0	0.14	766	0.20	0.08	
62.0	0.10	611	0.29	0.11	
67.0	0.028	1273	0.23	0.05	
72.5	0.031	519	0.31	0.13	

copyrite surface. For comparison a single electron transfer reaction such as,

$$Fe^{2+} \rightleftharpoons Fe^{3+} + e^-$$

at a Pt electrode at 25° C has a measured Tafel slope of 102 mV decade^{-1}, $n = 1$ and $\alpha = 0.58$ [11].

The reaction order with respect to various solution species for the anodic dissolution of p-type chalcopyrite was determined at 50°C in both 0.3 mol dm^{-3} HCl and 0.3 mol dm^{-3} H_2SO_4. The reaction order was determined by varying the concentration of the species of interest; e.g., H^+, while holding the concentration of all other species constant. The concentration of Fe^{+2}, Fe^{+3}, Cu^{+1} and Cu^{+2} were varied from 10^{-5}–10^{-2} mol dm^{-3}, and the concentrations of H^+ and Cl^- from 10^{-5} to 1.0 mol dm^{-3}. The slope of the plot log$I$ versus log$C$ at constant potential yields the reaction orders given below. The data indicate that the chalcopyrite dissolution reaction is virtually independent of H^+, Cl^-, Fe^{2+}, Fe^{3+}, Cu^{1+} and Cu^{2+} species in either sulphate or chloride media.

Species	*Reaction order, n*
H^+	$0 < n < 0.1$
Cl^-	$0 < n < 0.1$
Fe^{+2}	$0 < n < 0.2$
Fe^{+3}	$0 < n < 0.2$
Cu^{+1}	$0 < n < 0.2$
Cu^{+2}	$0 < n < 0.2$

The parameters as measured for the chalcopyrite dissolution are significantly influenced by the formation of the product layer. Low α values and high temperature-insensitive Tafel slopes have been found for a number of metals which under anodic potentials dissolve forming a product layer on the reaction surface. For example the valve metals dissolve in aqueous solvents to form metal oxide films [12], and lithium in propylene carbonate solvent forms a lithium carbonate product layer [13, 14]. Moreover with increasing thickness of product layers, Tafel slopes increase and α values decrease.

Ammou [3] in his study of the anodic dissolution of chalcopyrite in chloride media, suggested the formation of a product layer consisting of covellite (CuS) and elemental sulphur. The CuS which dissolves and reforms, resides in the pores of the elemental sulphur and thus inhibits the reaction at the chalcopyrite surface. Jones and Peters [4] also identified CuS as an intermediate product in their study of the anodic dissolution of chalcopyrite. Parker *et al.* [1, 2] studied the stoichiometry of the anodic dissolution of chalcopyrite using a ring-disc electrode. The results of

their experiments indicated that the formation of a gradually thickening layer of a copper-rich species on the surface was responsible for the slow passivation of the chalcopyrite surface during the first stage of oxidation. They suggested that the species might be a copper polysulphide, CuS_x ($x > 2$).

Although opinions vary as to the identity of the surface species, all workers [1–5] agree that the species remains on the surface and forms a barrier to electron transfer. The electrochemical dissolution of materials which form a product layer is often dominated by this layer of insoluble products. For chalcopyrite a layer of an iron deficient copper sulphide species could act as an interphase between the chalcopyrite and the solution and have the properties of a solid electrolyte; it is electronically insulating [12]. This 'Solid Electrolyte Interphase' (SEI) does, however, allow transference of ionic species from chalcopyrite to solution. Dissolution would occur by oxidation of the chalcopyrite and transport of iron and/or copper ions through the SEI to the solution. This product film is undoubtedly formed in part during equilibration of freshly polished chalcopyrite electrodes. The process of layer breakdown could be occurring partly in conjunction with the above chalcopyrite dissolution. Total film breakdown is a distinct possibility in the experimentally observed high current region at $E > 1.3$ V versus SHE.

3.3. *Application of galvanostatic pulse chronopotentiometry*

The anodic electrochemical dissolution reaction through a SEI is frequently limited by ionic transport with the largest fraction of the electrode overpotential developed on the SEI. Dissolution currents are described at high overpotentials by the equation [14]:

$$i_{act} = i_0 \exp\left(\frac{aZF\eta}{RTY}\right) = i_0 \exp\left(B\frac{\eta}{Y}\right) \quad (4)$$

where a is the half jump distance, Z the valence of the mobile ion, Y the layer thickness and B the electric field coefficient. This is a Tafel-like polarization dependence with a Tafel slope directly dependent upon temperature and layer thickness; i_0 is the zero field current density found from Tafel equations. However, the exponential dependence is an activation energy barrier for ion migration; i.e., an Arrhenius plot of this current i_0 yields the ΔH^0 for ionic migration. At low fields an ohm's law behaviour is found [14]:

$$i_{act} = 2i_0\frac{aZF\eta}{RTY} = \chi\frac{\eta}{Y} \quad (5)$$

where $2i_0aZF/RT$ is the conductivity (χ) of the SEI. Tables 2 and 3 list values of aZ/Y from both the low and high overpotential cases. These values obtained under different electric field conditions are similar, the discrepancy indicating possible film breakup and dissolution. Film thicknesses were estimated utilizing capacitance data collected from potential transients. The thickness of the anodically formed films can be derived using the following relation for two capacitors in series [14]:

$$Y = \frac{\sigma\epsilon}{0.113C} - \frac{Y'\epsilon}{\epsilon'} \quad (6)$$

where Y is the thickness of the film in A^0, $\epsilon = 10$ is assumed to be the dielectric constant of the film, ϵ' is the dielectric constant of the electrolyte, C = the capacitance of the chalcopyrite electrode in $\mu F\,cm^{-2}$, and σ is the roughness factor which to the first approximation = 1. Y' is the thickness of the Helmholtz layer which in concentrated aqueous solvent is approximated by the length of the dipole; since $Y'\epsilon \gg \epsilon'$ the second term in the above relation can be neglected. Capacitance data for the chalcopyrite electrodes were estimated

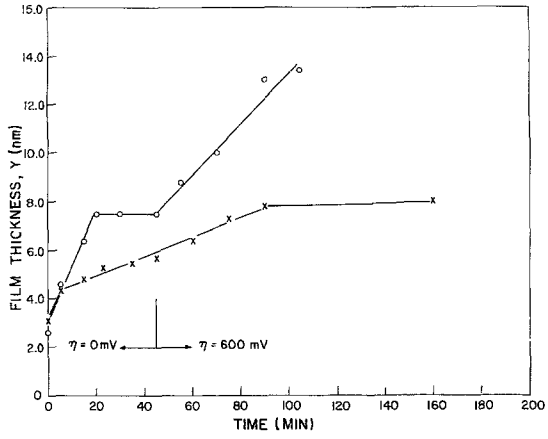

Fig. 9. Relationship between film thickness and time for chalcopyrite electrodes at 24°C. ○, 0.3 mol dm^{-3} HCl; ×, 0.3 mol dm^{-3} H_2SO_4.

Table 4. Anodic film characterization for the anodic dissolution of p-type chalcopyrite in 0.3 mol dm^{-3} HCl

T (°C)	C (μF cm^{-2})	Y (nm)	a_L (nm)	a_H (nm)	$B \times 10^6$ (cm V^{-1})	$\chi \times 10^9$ (ohm^{-1} cm^{-1})
0.3 mol dm^{-3} equilibrated electrode						
24	1.14	7.8	1.31	0.83	9.6	0.6
50	1.56	5.7	0.80	0.48	5.1	0.6
75	1.26	7.0	0.81	0.72	7.2	3.2
87	1.75	5.1	0.74	0.58	5.5	3.1
After 45 min anodic dissolution						
24	0.68	13.0	1.00	0.52	5.9	0.3
50	1.67	5.3	0.40	0.25	2.7	0.2
75	0.95	9.4	0.88	0.65	6.5	2.0
87	0.44	20.0	–	–	–	–

from the initial slopes of potential–time transients. Anodic galvanostatic pulses of 1 mA cm^{-2} and 100 μs duration were employed. Figure 9 depicts the relationship between film thickness and time.

Immersion of the polished electrode in the electrolyte and poising it at open circuit potential results in a rapid increase in film thickness. After 20 min., a constant thickness and rest potential are achieved. After 45 min. an overpotential of 600 mV was applied resulting in a further increase in film thickness. Tables 4 and 5 list film data collected for p-type chalcopyrite in 0.3 mol dm^{-3} HCl and 0.3 mol dm^{-3} H_2SO_4, respectively. Estimated film capacitance and thickness, as well as calculated barrier half jump distances for the low and high overpotential cases, electric field coefficients and conductivities are presented for the freshly polished and equilibrated electrodes and for electrodes on which a film was allowed to build-up over a 45 min. anodic dissolution period. Barrier half jump distances were calculated utilizing $2aZ/Y$ and aZ/Y values (see Tables 1 and 2) and assuming $Z = 3$. There appears to be no regular dependence of film thickness on temperature, film thickness does not always increase upon anodic dissolution. A significant blue-grey product layer was observed, however, but capacitance data show it to be very porous and not compact. Irregular temperature dependencies of barrier half jump distances, electric field coefficients and film conductivities suggest different film compositions at different temperatures. Values of the electric field

Table 5. Anodic film characterization for the anodic dissolution of p-type chalcopyrite in 0.3 mol dm^{-3} H_2SO_4

T (°C)	C (μF cm^{-2})	Y (nm)	a_L (nm)	a_H (nm)	$B \times 10^6$ (cm V^{-1})	$\chi \times 10^9$ (ohm^{-1} cm^{-1})
0.3 mol dm^{-3} equilibrated electrode						
24	1.56	5.7	0.50	0.42	4.9	1.6
34	1.67	5.3	0.33	0.37	4.2	0.4
52	1.47	6.0	0.50	0.34	3.7	0.4
75	1.62	5.7	0.74	0.57	5.7	2.6
87	1.69	5.2	0.94	0.69	6.7	0.9
After 45 min anodic dissolution						
24	1.14	7.8	0.23	0.16	1.8	0.6
34	1.27	7.3	0.37	0.27	3.1	0.4
52	0.23	9.6	0.32	0.26	2.9	0.4
73	1.56	5.7	0.29	0.25	2.5	0.1
87	1.54	5.7	–	–	–	–

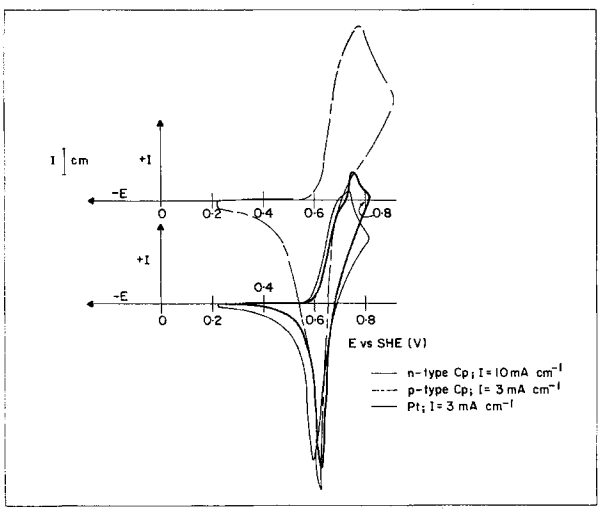

Fig. 10. Cyclic voltammograms obtained in 0.3 mol dm^{-3} HCl solutions with the I^-/I_3^- redox couple. 0.1 mol dm^{-3} KI–0.3 mol dm^{-3} HCl. Scan rate 0.1 V s^{-1}.

coefficient and film conductivity; i.e., $\simeq 5 \times 10^{-6}$ cm V^{-1} and about 1×10^{-9} ohm^{-1} cm^{-1} are similar to those found for typical barrier films [12, 14].

It is apparent that film formation occurs readily in both electrolytes on equilibration of freshly polished electrode surfaces. In particular the film acts as a solid electrolyte interphase as indicated by the low electrode interfacial capacitance ($<2\,\mu F\,cm^{-2}$) as compared to the expected double layer capacitance of about $20\,\mu F\,cm^{-2}$ for an electrode without a product film [13].

3.4. *Electron transfer to various redox couples*

The nature of the product layer resulting from the anodic dissolution of chalcopyrite was further investigated by studying the rate of electron transfer from various redox couples, I^-/I_3^-, Fe^{2+}/Fe^{3+}, Cu^+/Cu^{2+}, to the surface layer. The experimental work was done using the cyclic voltammetry technique to compare the electron transfer from the redox couples to Pt, n-type (Timmins) chalcopyrite and p-type (Transvaal) chalcopyrite. The electrodes were equilibrated in the 0.3 mol dm^{-3} HCl solutions containing the respective redox couples for 10 min before the repetitive cyclic scans were performed at room temperature.

Figure 10 shows the cyclic voltammogram obtained from 0.3 mol dm^{-3} HCl electrolyte containing the I^-/I_3^- couple. This couple behaves with the same degree of reversibility at all three

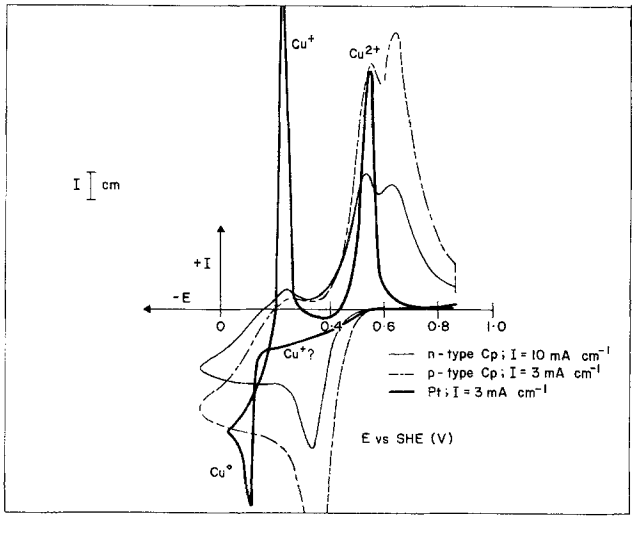

Fig. 11. Cyclic voltammograms obtained in 0.3 mol dm^{-3} HCl solutions with the Cu^{2+}/Cu^+ and Cu^+/Cu^0 redox couples. 0.1 mol dm^{-3} Cu^{2+}–0.3 mol dm^{-3} HCl. Scan rate 0.1 V s^{-1}.

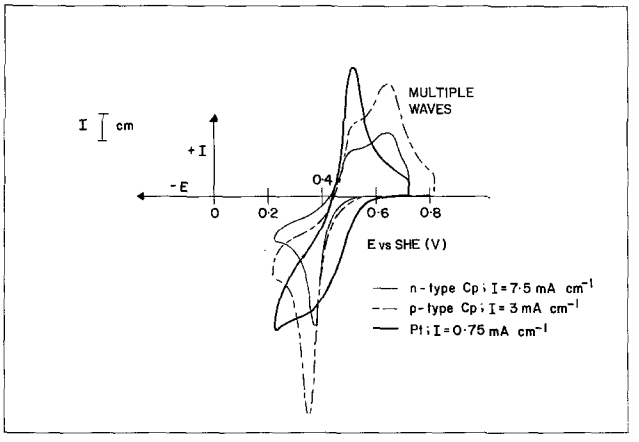

Fig. 12. Cyclic voltammograms obtained in in 0.3 mol dm^{-3} HCl solutions with the Cu^{2+}/Cu^{+} redox couple. Elemental copper was not formed in these tests. Scan rate 0.1 V s^{-1}.

electrodes. Much higher currents are obtained at the n-type chalcopyrite surface than at the p-type chalcopyrite surface; this could be due in part to the significantly higher bulk resistivity of the p-type electrode (see Table 1) or more likely to a higher conductivity of the SEI on n-type chalcopyrite. At the imposed potentials, both chalcopyrite electrodes are degenerate and act like metals with respect to electron transfer.

Figure 11 shows the cyclic voltammograms obtained from 0.3 mol dm^{-3} HCl containing the Cu^{2+}/Cu^{+} and Cu^{+}/Cu^{0} couples. At the Pt surface, the Cu^{+} is reduced to Cu^{0} followed by the sequence $Cu^{0} \rightarrow Cu^{+} \rightarrow Cu^{2+}$ as the scan goes anodic; note that the reaction $Cu^{2+} \rightarrow Cu^{+}$ does not appear to occur to any great extent on Pt; i.e., Cu^{2+}/Cu^{+} is not reversible under these conditions. On n- and p-type chalcopyrites the Cu^{2+}/Cu^{+} couple is more reversible than on Pt, but reduction of Cu^{+} to Cu^{0} occurs to a small extent. On the chalcopyrite electrodes the oxidation wave $Cu^{+} \rightarrow Cu^{2+}$ shows two peaks, suggesting that different Cu^{+} chloro-complexes are being oxidized. The enhanced currents, multiple waves and little reduction to Cu^{0} observed at the chalcopyrite electrodes suggest interaction of the ionic copper species with the chalcopyrite SEI.

The cyclic voltammograms shown in Fig. 12 are the same electrodes and electrolyte systems as shown in Fig. 11, but in this case, the cathodic scan is stopped before the potential becomes cathodic enough to form Cu^{0}. This demonstrates clearly that the Cu^{2+}/Cu^{+} couple is more reversible and gives higher currents on chalcopyrite than on Pt. The multiple anodic peaks occur in the potential region where the chalcopyrite electrode produces negligible currents in the absence of redox couples.

Figure 13 shows the cyclic voltammograms obtained from 0.3 mol dm^{-3} electrolyte containing the Fe^{3+}/Fe^{2+} redox couple. The results indicate that:

1. The Fe^{3+}/Fe^{2+} couple is not as reversible as the I^{-}/I_3^{-} and Cu^{2+}/Cu^{+} couples;

2. The Fe^{3+}/Fe^{2+} is as reversible on n-type chalcopyrite as it is on Pt; however, the currents obtained at Pt are greater than those obtained at n-type chalcopyrite;

3. p-type chalcopyrite yields negligible currents under these conditions; i.e., the Fe^{2+}/Fe^{3+} couple is much less reversible on p-type chalcopyrite in

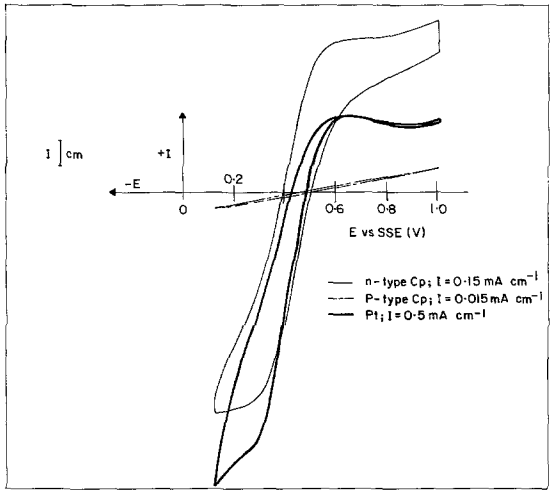

Fig. 13. Cyclic voltammograms obtained in 0.3 mol dm^{-3} HCl solutions containing the Fe^{3+}/Fe^{2+} redox couple. 0.1 mol dm^{-3} Fe^{3+}, 0.1 mol dm^{-3} Fe^{2+}. Scan rate 0.1 V s^{-1}.

the potential region where electron transfer readily occurs to the I^-/I_3^- and Cu^{2+}/Cu^+ redox couples.

Parker *et al.* [1, 2] observed that the Fe^{3+}/Fe^{2+} couple (especially as sulphate) was much less reversible on corroding chalcopyrite than on pyrite or platinum, in agreement with the results observed in this work. They further observed that the couples Cu^{2+}/Cu^+ and I^-/I_3^- were more reversible than Fe^{3+}/Fe^{2+}, and that all couples were much less reversible on chalcopyrite than on pyrite.

Together these data indicate that the Cu^{2+}/Cu^+ and I^-/I_3^- species can interact with the chalcopyrite reaction surface to allow facile electron transfer to occur. The Fe^{3+}/Fe^{2+} species particularly in the case of p-type chalcopyrite and to a lesser extent with n-type chalcopyrite are not able to effect this and indeed passivate the surface towards electron transfer.

The nature of ionic interactions of cations and anions with the surface of the SEI are such that the conductivity of the SEI is modified either by incorporation of the cations or anions in the layer interphase or, in the case of an increase in the conductivity, by breaking down this insulating layer by chemical oxidation.

3.5. *Chemical leaching experiments*

The results presented above have shown the importance of electrochemical reactions during the initial (< 10 nm) leaching of chalcopyrite, and have indicated significant differences in the ease of electron transfer in the presence of various redox couples. To see if such effects persist during the long time bulk chemical leaching of $CuFeS_2$, the Transvaal chalcopyrite was leached in the presence of various oxidants. Figure 14 shows the resulting initial rate constants for the chemical leaching of chalcopyrite plotted against the oxidation potential of the solution as measured at 90° C on a chalcopyrite electrode. As suggested by the electrochemical experiments (Figs. 1 and 5), the bulk leaching rate shows a global tendency to increase with increasing oxidation potential. The rate in bromate solutions ($E = 0.8$–0.95 V versus SHE) is some two orders of magnitude greater than in ferric sulphate media ($E = 0.6$–0.8 V versus SHE). Also, for each individual oxidant, the rate increases as the oxidation potential increases.

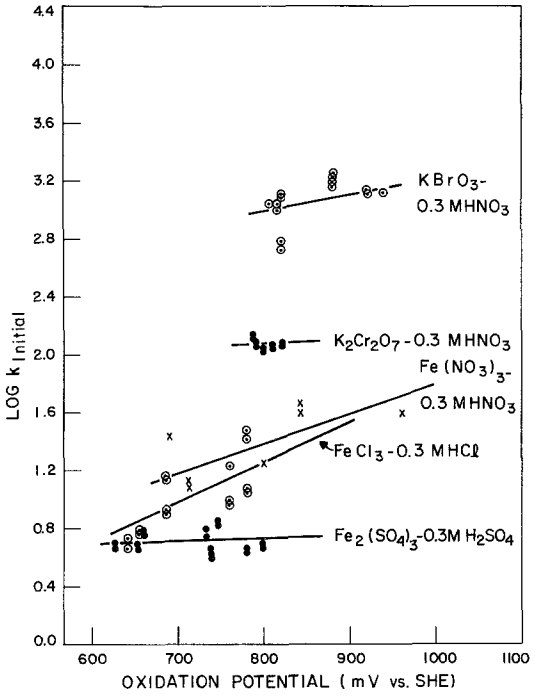

Fig. 14. The effect of solution oxidation potential on the rate of chemical leaching of chalcopyrite by various oxidants. 1 g Transvaal chalcopyrite, 90° C.

These two observations suggest that electrochemical factors are still of considerable significance in controlling the rate of bulk dissolution of chalcopyrite. There are, however, a number of features which indicate that other effects, not directly related to simple oxidation potential, are equally important. For example, it is possible to have different oxidants with essentially the same oxidation potential that yield quite different leaching rates. This is especially evident for ferric ion leaching where at a given potential the order of the rate of reaction is:

$$Fe(NO_3)_3 > FeCl_3 > Fe_2(SO_4)_3.$$

These reactions have a number of common features including elemental sulphur formation [9], but they yield different leaching rates, and the differences cannot be related to oxidation potential differences only. This fact is demonstrated by the different effects of oxidation potential on the rate for the various oxidants. For the more powerful oxidizing agents such as $K_2Cr_2O_7$ and $KBrO_3$, the sulphide is oxidized to sulphate, and the elimination of the sulphur layer may be partly res-

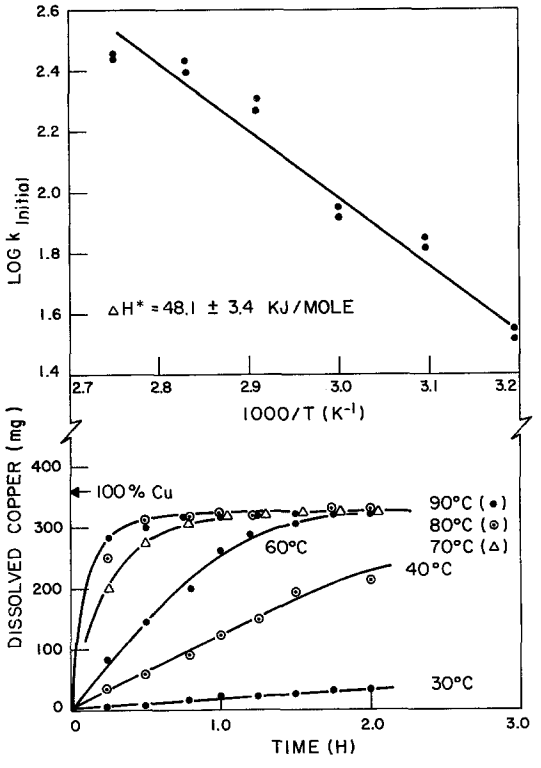

Fig. 15. Leaching curves and Arrhenius plot for the chemical dissolution of 1 g Transvaal chalcopyrite in 0.1 mol dm^{-3} $KBrO_3$–0.3 mol dm^{-3} HNO_3 media.

ponsible for the enhanced bulk chemical leaching. Virtually identical curves were produced using the oxidation potentials recorded on Pt at 90° C, except that the graph was displaced by 300–400 mV.

As remarked previously, the activation energies for the chemical leaching of chalcopyrite in $FeCl_3$–HCl or $Fe_2(SO_4)_2$–H_2SO_4 media are similar to the values found for the anodic dissolution in HCl or H_2SO_4 solutions, respectively. Figure 15 shows that similar activation energies ($\simeq$ 50 kJ mole^{-1}) are found even for the most potent oxidants such as $KBrO_3$, and the similar activation energies noted for all the oxidants again suggest that a common underlying mechanism plays an important role in all the systems.

4. Conclusions

The application of the double potential pulse chronoamperometry technique to the study of the anodic dissolution of chalcopyrite in 0.3 mol dm^{-3} HCl and 0.3 mol dm^{-3} H_2SO_4 has indicated that a surface layer SEI is formed which slows the rate of electron transfer and, hence, the dissolution rate. The higher Tafel slopes and anomalous Arrhenius behaviour obtained in 0.3 mol dm^{-3} H_2SO_4 suggest that the surface layer formed in that medium is different from that produced in 0.3 mol dm^{-3} HCl electrolyte.

The rate of electron transfer from various redox couples to the surface layer formed on chalcopyrite in 0.3 mol dm^{-3} HCl electrolyte was investigated using the technique of cyclic voltammetry. The results indicated that the Fe^{3+}/Fe^{2+} redox couple was not as reversible as the Cu^{2+}/Cu^{+} and I^-/I_3^- redox couples in general, and that the Fe^{3+}/Fe^{2+} couple is much less reversible on p-type chalcopyrite in the potential region where electron transfer readily occurs to the I^-/I_3^- and Cu^{2+}/Cu^{+} redox couples.

Chemical leaching experiments using oxidants with different oxidation potentials have confirmed the important role of electrochemical effects in the bulk leaching of chalcopyrite. The results also indicated that other factors such as the nature of the surface films, transport phenomena, etc. were equally important for the long term chemical leaching of $CuFeS_2$. The activation energies for the chemical leaching in the presence of oxidants, including $KBrO_3$, are in the range 48–72 kJ mole^{-1}, and this suggests common underlying mechanisms in all the systems.

Acknowledgements

One of the authors (RSM) received financial support in the form of a Visiting Fellowship from the National Sciences and Engineering Research Council of Canada. The assistance of D. J. Hardy with the chemical leaching experiments is also recognized.

References

[1] A. J. Parker, R. L. Paul and G. P. Power, *Aust. J. Chem.* **34** (1981) 13.
[2] *Idem, J. Electroanal. Chem.* **118** (1981) 305.
[3] M. Ammou-Chokroum, P. K. Sen and F. Fouques, Developments in Mineral Processing, in 'Proceedings, 13th International Minerals Processing Congress', Part A, Warsaw, Poland, June 1979 (edited by J. Laskowski) Elsevier Scientific Publishing Co., New York (1981) pp. 759–809.
[4] D. L. Jones and E. Peters, Int. Corr. Conf. Ser.

1973, NACE-4, (1977) pp. 443–458.
[5] G. W. Warren, PhD thesis, University of Utah (1978).
[6] H. G. Linge, *Hydrometallurgy*, **2** (1976) 51.
[7] J. P. Bauer, H. L. Gibbs and M. E. Wadsworth, Paper 72-B-96, Annual AIME meeting, San Francisco (1972).
[8] '1980 Annual Book of ASTM Standards', American Society for Testing Materials, Philadelphia (1980).
[9] J. E. Dutrizac, *Metall. Trans.* **12B** (1981) 371.
[10] D. D. MacDonald, 'Transient Techniques in Electrochemistry', Plenum Press, New York (1977).
[11] J. O'M. Bockris and A. K. N. Reddy, 'Modern Electrochemistry', Vol. 2, Plenum Press, New York (1970).
[12] L. Young, 'Anodic Oxide Films', Academic Press, London (1961).
[13] E. Peled, *J. Electrochem. Soc.* **126** (1979) 2047.
[14] E. B. Yeager, B. Schumm, Sr, G. Blomgren, D. R. Blankenship, V. Leger and J. Akridge, (Eds.), 'Lithium Nonaqueous Battery Electrochemistry', Electrochemical Society Inc., Pennington, New Jersey (1980) pp. 115–29.